ARTICLE

The fate of organic species upon sintering of thiol-stabilized gold nanoparticles under different atmospheric conditions

Received 00th January 20xx,
Accepted 00th January 20xx

DOI: 10.1039/x0xx00000x

Paige K. Summers[a], Alexander Angeloski[a,b], Richard Wuhrer[c], Michael B. Cortie[d], Andrew M. McDonagh*[a]

Understanding and controlling the sintering behavior of gold nanoparticles is important for applications such as printed electronics, catalysis and sensing that utilize these materials. Here we examine the processes by which thiol-protected gold nanoparticles thermally sinter under a variety of atmospheres. We find that upon sintering, the surface-bound thiyl ligands exclusively form the corresponding disulfide species when released from the gold surface. Experiments conducted using air, hydrogen, nitrogen, or argon atmospheres revealed no significant differences between the temperatures of the sintering event nor on the composition of released organic species. When conducted under high vacuum, the sintering event occurred at lower temperatures compared to ambient pressures in cases where the resulting disulfide had relatively high volatility (dibutyl disulfide). Hexadecylthiol-stabilized particles exhibited no significant differences in the temperatures of the sintering event under ambient pressures compared to high vacuum conditions. We attribute this to the relatively low volatility of the resultant dihexadecyl disulfide product.

Introduction

Gold nanoparticles (AuNPs) have attracted significant attention due to their unique properties and diverse applications.[1, 2] AuNPs may be sintered to form continuous, electrically conducting gold films at moderate to low temperatures.[3, 4] In contrast, for many sensing and catalysis applications it is crucial to prevent sintering and thereby maintain the size and shape of the nanoparticles.[5-7] Understanding the mechanism of the sintering process as well as the influence of atmosphere and ligands on the thermal stability of AuNPs can provide strategies to prevent, control or induce sintering for various applications such as sensors, radio frequency identification tags and in bioimaging.[8-10]

Sintering may be defined as "*temperature-induced coalescence and densification of porous solid particles below the melting points of their major components*"[11] and for AuNPs with diameters >1.5 nm, the temperatures applied to induce sintering are generally significantly lower than the NP melting points.[12] However, a thin molten surface layer between actively coalescing particles has been described.[13] Coalescence (the disappearance of the boundaries between particles) of organic molecule-stabilised AuNPs generally starts with contact between the NPs and subsequent neck formation.[14] As the surface area of the merging nanoparticles decreases, surface energy is transformed into thermal energy, thus increasing the temperature of the particles.[15, 16]

There remains considerable debate about whether stabilising ligands should first be released from the gold surface[17-19] or if sintering can proceed with the surface layer intact.[20-23] Although the thermal stability and desorption of thiol-based monolayers on flat gold surfaces has been reasonably well investigated, few reports have examined this behaviour on the surfaces of AuNPs.[24-30] Such knowledge is important as the desorption behaviour directly affects the sintering temperatures of AuNPs.[31] In the context of self-assembled monolayers (SAMs), Reimers et al. describe an equilibrium between surface-bound thiyl species (that is, Au(0)-˙SR species bonded via strong van der Waals attractions, polarization effects and s–d hybridization) and unbound disulfide compounds.[32] This model improves upon the more classical Au(I)-thiolate model for Au-SR compounds (such AuNPs). Considering the model of Reimers et al, one might predict that species of the type RS-SR might predominate when released from gold surfaces. Desorption studies on SAMs using hexanethiol on Au(111) under high vacuum at room temperature support this equilibrium model[29] and the disulfide derived from the stabilising thiol has been found to be the major species desorbed from SAMs on gold surfaces upon heating under particular conditions.[33]

[a] *School of Mathematical and Physical Sciences, University of Technology Sydney, Broadway, Ultimo, NSW 2007, Australia.*
[b] *Australian Centre for Neutron Scattering, Australian Nuclear Science and Technology Organisation, Kirrawee DC, NSW, 2232, Australia*
[c] *Advanced Materials Characterisation Facility (AMCF), Western Sydney University, Locked Bag 1797, Penrith, NSW, 2751, Australia.*
[d] *School of Mechanical, Materials, Mechatronics and Biomedical Engineering, University of Wollongong, Northfields Ave, Wollongong, NSW 2522, Australia*

Electronic Supplementary Information (ESI) available: TEM micrographs, 1H NMR spectra, TGA-MS data, and statistical analysis of sintering data. See DOI: 10.1039/x0xx00000x

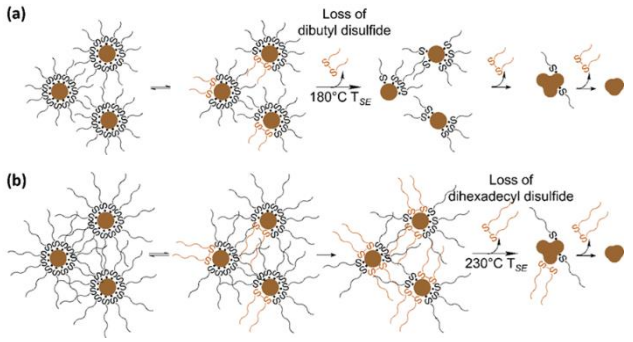

Fig. 1 Schematic depicting the removal of short (a) and long (b) chain thiyl bound ligands from the surface of gold nanoparticles under ambient pressures. Initially, an equilibrium exists between bound thiyl and disulfide. (a) Short chain butanethiyl produces volatile dibutyl disulfide that leave the vicinity of the particle surface at moderate temperatures. (b) Long chained hexadecanethiyl ligands produce dihexadecyl disulfide with relatively low volatility that leave the surface at significantly higher temperatures.

In gold clusters stabilized using thiols, Au-S bonds can be cleaved at temperatures where the ligands remain in the vicinity of the particle prior to the sintering event.[34] Smith and Hutchison provided evidence that disulfide compounds (formed from the stabilising thiol compound) exist on the surface of AuNPs at room temperature and that their concentration increased upon heating.[35] Disulfide species have also been identified in the ligand shell of thiolate-stabilised Au_{130} clusters.[36] These observations are not inconsistent with the concept of an equilibrium between bound thiyl and disulfide species. We hypothesized that such an equilibrium would be disrupted when the disulfide leaves the vicinity of the particle surface, which will be a function of the disulfide volatility.

Ligands have a significant role in the stability of AuNPs, with longer chain alkanethiol ligands (thus lower volatility) generally exhibiting a greater temperature of the sintering event (TSE) compared to shorter chain (higher volatility) ligands.[9, 31, 35, 37, 38] Here we show that the sintering of thiol-stabilized AuNPs is critically controlled by the equilibrium between thiyl and disulfide species and describe the influence of ligand volatility and atmosphere (Fig. 1). We explore the sintering of thiol-stabilized AuNPs using ^{1}H nuclear magnetic resonance spectroscopy, themogravimetric analysis, differential scanning calorimetry, electrical conductivity measurements, and mass spectrometry to elucidate the processes that occur under different atmospheric conditions during the thermal sintering event, and examine the nature of the residual material upon sintering. These findings shed new light on the processes involved in sintering alkanethiol-stablized AuNPs.

Experimental

General

1-Butanethiol (Sigma-Aldrich), 1-hexadecanethiol (Fluka), and deuterated chloroform ($CDCl_3$) were used as received. Tetrachloroauric acid[39], butanethiol-capped AuNPs (BT@AuNPs), and hexadecanethiol-capped AuNPS (HDT@AuNPs) were prepared using literature procedures.[40] Dihexadecyl disulfide and dibutyl disulfide were synthesised using literature procedures.[33] Proton nuclear magnetic resonance (^{1}H NMR) spectra were recorded using an Agilent NMR spectrometer operating at 500.13 MHz ($CDCl_3$, δ7.26). Themogravimetric analysis-mass spectroscopy (TGA-MS) analysis was performed using a Netzsch STA 449 F5 Jupiter TGA instrument coupled to an Agilent 5977B mass spectrometer. The heating rate was 10 °C min^{-1} under a 30:70 helium: air gas flow rate of 50 ml/min, using 5-6 mg of the sample in an alumina oxide crucible. Themogravimetric analysis (TGA) was performed using a TA Instruments SDT Q600 with a heating rate of 10 °C min^{-1} under an air atmosphere and flow rate of 50 ml/min with 5-6 mg of sample used. Differential scanning calorimetry (DSC) was completed using a TA Instruments Q2000 with a heating rate of 10 °C min^{-1}. Samples were prepared in air in a Tzero pan with Tzero hermetic lid, which could be punctured using a steel pin.

Transmission electron microscopy (TEM) images were taken using a FEI Tecnai T20 TWIN microscope (LaB6) operating at 200 keV and fitted with a Gatan 894 2k x 2k camera. The TEM samples were prepared by evaporating diluted nanoparticle solution on the carbon-coated copper grid. The images were analysed using ImageJ software (https://imagej.nih.gov/ij/). Scanning electron microscopy (SEM) was performed at facilities at Western Sydney University. A Zeiss Merlin field emission gun scanning electron microscope (FEGSEM) was utilised for imaging samples prepared on stubs. The FEGSEM was operated at 20kV accelerating voltage in Hivac mode at a working distance of approximately 3 mm. Both secondary and in-lens secondary detectors were utilised for imaging.

Resistance measurements of AuNP films

Films of AuNPs were formed by drop casting 10 mg/mL suspensions of AuNPs in chloroform onto DropSens (Metrohm) interdigitated gold electrodes and heated within a modified Linkam THMS600 temperature control stage. A heating rate of 10 °C min^{-1} from room temperature to 350 °C was maintained using a Linkam TMS 94 controller. The temperature was measured using a Rigol DM3058E digital multimeter and a PT100 (RS PRO) RTD sensor, 2mm x 5mm Class B thermocouple placed within 2 mm of the gold electrodes and held in contact with the heating block surface using a small clamp. We note that temperature measurements using a thermocouple in vacuo can be problematic and so data were verified using certified melting standards (acetanilide, saccharin, dicyandiamide, benzanilide, acetaminosalol, phenacetin, benzil, azobenzene and benzoic acid).

Electrical resistance was measured with a Rigol DM3068 digital multimeter (maximum resistance of 100 MΩ). A LabView program was used to interface with and control the multimeters, and to acquire the temperature and electrical resistance. The flow rate of gases was controlled using an Apex mass flow controller with a rate of 25 ml/min. High vacuum measurements were recorded using a highly modified Linkam heating stage mounted within a purpose-built vacuum chamber operating at ~8 x 10^{-6} mbar. Data were analysed using Jamovi software (https://www.jamovi.org/) with Kruskal-Wallis One-

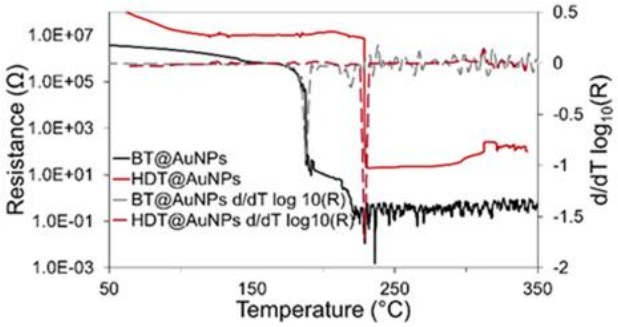

Fig. 2 Representative resistance data obtained from films of BT@AuNPs and HDT@AuNPs during heating in air.

Way ANOVA (non-parametic) and Dwass-Steel-Critchlow-Fligner pairwise comparisons to calculate p-values.

Analysis of heated AuNPs

AuNPs were heated in gastight conical reaction vials to 300 °C under atmospheres of air, nitrogen or hydrogen. The organic residues were collected by rinsing the interior of the cooled vials with deuterated chloroform and then filtering through cellulose fibre (Kimwipe) to remove elemental gold. The resultant solutions were analysed using ^{1}H NMR spectroscopy.

Results and Discussion

AuNPs were synthesized using variations of the two-phase Brust-Schiffrin method.[32] BT@AuNPs (synthesized using 1-butanethiol as stabilising ligand) had diameters of 3.2 (± 0.1) nm (measured using TEM, Fig. S1). HDT@AuNPs (synthesized using 1- hexadecanethiol as stabilising ligand) had diameters of 2.7 (± 0.05) nm (Fig. S1). The ^{1}H NMR spectra of BT@AuNPs and HDT@AuNPs in $CDCl_3$ (Fig. S2) are similar to previously reported spectra of octanethiol-stabilized AuNPs.[35] In the ^{1}H NMR spectrum of BT@AuNPs, no signals arising from the protons attached to C1 were observed. This has been reported for thiol-stabilized AuNPs with diameters of ~3 nm.[41-43] However, in small clusters with diameters of ~1 nm, NMR signals arising from the alpha protons were observed.[44, 45] This was attributed to fewer types of binding sites on the small clusters, thus diminishing spectral broadening created from chemical shift distributions. Furthermore, methylene groups close to the Au surface are more densely packed relative to those further from the surface and therefore experience faster spin relaxation from dipolar interactions[42] resulting broader signals. The resonances for the protons attached to C2 to C3 are observed as a broad peak from 1.45-1.10 ppm, and a triplet at 0.88 ppm. The ^{1}H NMR spectrum of HDT@AuNPs contains a signal at 1.60 ppm assigned to the protons attached to C2, a broad peak at 1.26 ppm assigned to protons attached to C3-15, and a triplet at 0.88 ppm assigned to the protons on C16. No signals arising from unbound thiol were observed.

The AuNPs were heated at a rate of 10 °C min^{-1} in air to 350 °C to facilitate sintering. Figure S3 shows representative SEM images of (a) as-prepared BT@AuNPs and (b) sintered BT@AuNPs. Prior to sintering (Fig. S3a/c), the nanoparticulate nature of the samples is apparent whereas after sintering (Fig. S3b/d), no nanoparticles are evident but larger gold structures separated by grain boundaries are observed. It has been reported that there is a kinetic component to the thermal sintering of the AuNPs, with slower heating rates leading to lower temperatures of sintering events.[46] Thus, a heating rate of 10 °C min^{-1} was maintained for all experiments to allow for meaningful comparisons to be made.

The resistances of drop-cast films of AuNPs were measured as a function of temperature using interdigitated gold electrodes heated at a rate of 10 °C min^{-1}. The sintering event is characterized by a drop in resistance from values >1 MΩ to values <100 Ω. We use the definition of the temperature of the sintering event (T_{SE}) as the temperature at the maximum rate of change in resistance.[10] Figure 2 shows representative data recorded while heating BT@AuNPs and HDT@AuNPs. Resistance at room temperature was significantly lower for films of BT@AuNPs compared to those of HDT@AuNPs. The greater T_{SE} for the longer chain length HDT@AuNPs compared to BT@AuNPs is consistent with previous data (230 °C and 180 °C respectively).[31]

This ligand effect has also been observed by others investigating AuNPs stabilized using alkanethiol compounds.[47-49] Low-polarity alkyl groups have been reported to not disturb the gold core framework significantly[50] and longer alkane chains have been shown to increase T_{SE}, indicating that interactions between the alkyl chains contribute to the observed trend in T_{SE}.

TGA-MS data (see Fig. S4) were collected for BT@AuNPs at temperatures between 40 °C and 1300 °C. Upon heating BT@AuNPs under He or air atmospheres, no species were detected prior to the main mass loss event. A mass loss of ~10 % was observed and occurred at the T_{SE}, which is consistent with previous reports.[35] In He or air atmospheres, the mass spectrometry data revealed a single peak in the extracted ion chromatogram. Analysis of the chromatogram showed mass spectra that corresponded to only dibutyl disulfide. No other products were detected. Products formed from heating HDT@AuNPs were not detected due to their low volatility and thus precluded MS analysis.

The nature of the compound(s) released from the surface before and during the sintering event is crucial to the understanding of the processes involved with sintering of thiol-stabilized AuNPs. To obtain this data, ^{1}H NMR spectra were collected of the residues of AuNPs heated at 10 °C min^{-1} beyond the T_{SE} in airtight reaction vessels (Fig. 3). After cooling to room temperature, solvent ($CDCl_3$) was added to the reaction vessels, filtered to remove the sintered gold, and ^{1}H NMR spectra recorded immediately. Figure 3a shows the ^{1}H NMR spectrum of BT@AuNP residue post-sintering. Comparison with an authentic sample of dibutyl disulfide reveals that the major reaction product is disulfide. HDT@AuNPs exhibited the same behavior (Fig. 3b). This is in agreement with previous reports that describe the mechanism of the removal of thiol-based ligands from SAMS by oxidation of the surface-bound thiyls to the corresponding disulfide compounds.[29] The ^{1}H NMR spectra of other possible sulphur-containing compounds 1-butanethiol and di-n-butylsulfide differ from those shown in Figure 3 as (in deuterated chloroform) the signals of the protons bonded to α-

carbon atoms have chemical shifts at ~2.5 ppm[51] while peaks at for the dialkyl disulfide compounds are observed at ~2.7ppm (Fig. S5).

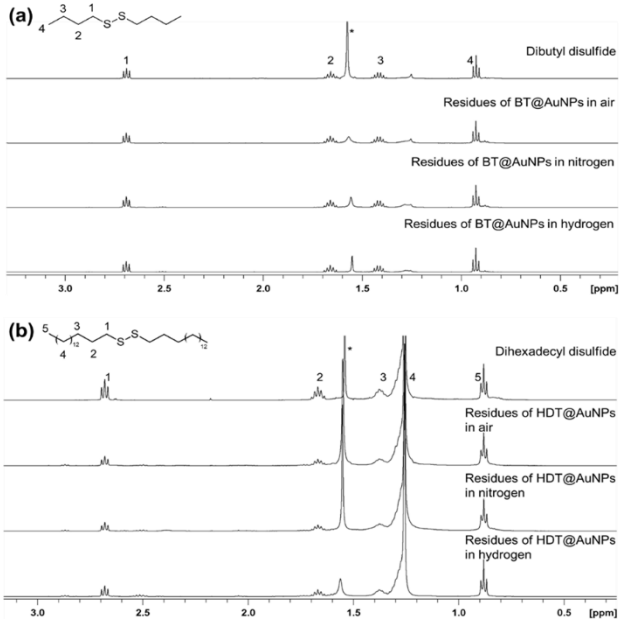

Fig. 3 ^{1}H NMR spectra of sintering residue of (a) BT@AuNP in hydrogen and nitrogen and (b) HDT@AuNP in hydrogen and nitrogen (* denotes H_2O at 1.58 ppm).

Comparison of TGA data for the AuNPs with data for dibutyl disulfides and dihexadecyl disulfide is informative. Thermogravimetry with a heating rate of 10 °C min-1 from room temperature to 450 °C, Figure 4, shows mass losses of 8 % and 33 % for BT@AuNPs and HDT@AuNPs, respectively, which is in agreement with previously reported literature.10 Interestingly, total mass loss of neat dibutyl disulfide occurs at a temperature ~50°C lower than the temperature of mass loss from BT@AuNPs. In contrast, mass loss for neat dihexadecyl disulfide occurs at similar temperatures to that of HDT@AuNPs. That is, for BT@AuNPs, the ligands remain in the vicinity of the AuNPs at temperatures beyond those where neat dibutyl disulfide vaporizes. On the other hand, dihexadecyl disulfide vaporizes at a temperature more than 100 °C greater than that of dibutyl disulfide (significantly greater van der Waals interactions due to longer chain lengths) and so for the HDT@AuNPs, the long-chain intermolecular interactions between the ligands have a more dominant effect on TSE. In general, it is apparent that the volatility of the disulfide has a significant effect on the temperatures at which ligands are removed from the particle environment.

The thermal behavior of the AuNPs was also examined using DSC (Fig. 5). Samples were placed in DSC pans where the hermetic seals were either intact (closed pan) or punctured (open pan). Figure 5 shows a difference of ~20 °C in the temperatures of maximum heat flow (associated with the sintering event) for BT@AuNP in open pan (200 °C) and closed pan (220 °C) experiments. For HDT@AuNPs, the open and closed pan experiments showed no difference in the temperature of maximum heat flow with sharp peaks at 233 °C for both.

The DSC results suggest that when BT@AuNPs are heated in an environment where the disulfide product can readily escape, the equilibrium (as depicted in Figure 1) is shifted to the right

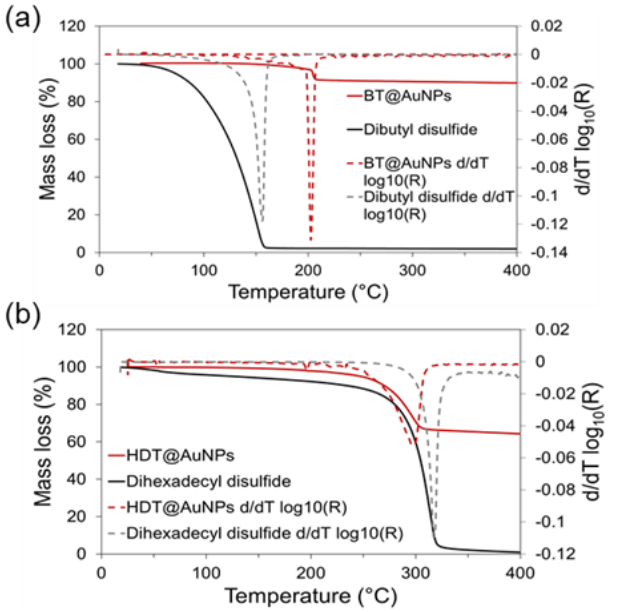

Fig. 4 Themogravimetric analysis data for (a) BT@AuNPs and dibutyl disulfide and (b) HDT@AuNPs and dihexadecyl disulfide

relative to the case where the BT@AuNPs are heated in a closed environment and the disulfide is prevented from escaping. In contrast, the different pan environments have minimal effect on HDT@AuNPs sintering event, as the dihexadecyl disulfide has relatively low volatility, as shown in Figure 5, and thus the amount that remains in the vicinity of the NPs is unaltered.

AuNPs were sintered under different gaseous atmospheres and electrical resistance data were used to determine the TSE (Table 1). These data are consistent with the TGA data. The Kruskal-Wallis (non-parametric) method was used to compare TSE data obtained under different gaseous environments (Tables S1 & 2). No significant differences ($p>0.05$) in TSE were observed for the different gaseous environments for BT@AuNPs or HDT@AuNPs, respectively. That is, oxygen-containing, hydrogen, or inert atmospheres exert no influence on the sintering event or the temperature-induced ligand reaction.

Coupled with the TGA data (Fig. 4), it is apparent that, at the TSE for HDT@AuNPs, significant amounts of dihexadecyl disulfide remain in the vicinity of the sintered gold up until ~320 °C. In the case of BT@AuNPs, removal of dibutyl disulfide at the TSE was rapid as this species volatilizes at temperatures less than

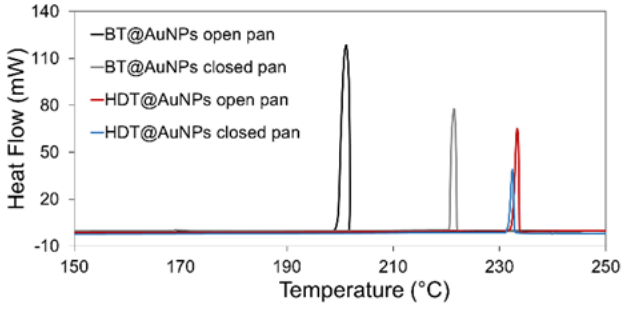

Fig. 5 Heat flow peaks (exothermic) under sealed and open environments for BT@AuNP and HDT@AuNP.

Table 1 Summary of TSE (°C) of BT@AuNP and HDT@AuNP determined using electrical resistance measurements in different atmospheres.

AuNPs	Air	Nitrogen	Argon	Hydrogen	Vacuum
BT@AuNPs	184 (±4)	190 (±1)	187 (±7)	192 (±12)	152 (±4)
HDT@AuNPs	215 (±9)	218 (±9)	218 (±18)	213 (±12)	206 (±4)

the TSE. Visual observation of the HDT@AuNPs during sintering revealed that the gold becomes lustrous only above the temperature of complete volatilisation of the dihexadecyl disulfide, whilst BT@AuNPs formed lustrous films at the TSE. Comparison of TSE data for HDT@AuNPs sintered under gaseous atmospheres compared to in vacuo (~8 x 10-6 mbar) also showed no significant differences ($p>0.05$). In contrast, TSE data for BT@AuNPs sintered in vacuo were significantly lower ($p<0.05$) compared to TSE under the gaseous environments. BT@AuNPs sintered ~30 °C lower under high vacuum compared to BT@AuNPs under the gaseous environmental conditions. We attribute this difference to the greater volatility of the dibutyl disulfide in vacuo compared to atmospheric pressure, which has the effect of moving the equilibrium (shown in Figure 1) to the right.

This effect was also observed in the open/closed DSC measurements. This effect is not evident in the TSE data for the HDT@AuNPs because of the much lower volatility of the dihexadecyl disulfide (compared to dibutyl disulfide). These observations are consistent with those from open/closed pan DSC and TGA data.

We have also considered the possibility that the transport of detached species to the gas phase may be more efficient in the presence of gas flux than in vacuum. However, this effect would show the opposite trend to that observed. Processes involved with sintering of BT@AuNPs and HDT@AuNPs were investigated under different atmospheric conditions. The organic residue obtained upon sintering thiol-stabilized AuNPs was unambiguously identified as the dialkyl disulfide and was formed consistently regardless of the atmospheric conditions. Furthermore, the various gaseous atmospheres had no significant effect on T_{SE} for either the BT@AuNPs or HDT@AuNPs.

Conclusions

TGA data showed that neat dibutyl disulfide evaporated well before the T_{SE} of BT@AuNP, however TGA-MS of BT@AuNP. showed no loss of dibutyl disulfide before T_{SE}. If the Au-S interaction was the dominant factor that influenced the T_{SE}, then applying high vacuum should result in no change the T_{SE}. We showed that this is not the case and that sintering under high vacuum conditions resulted in significantly lower T_{SE}. This can be explained by considering an equilibrium between dibutyl disulfide (the only detected volatile species) and the bound thiyl. Increasing the rate of removal of disulfide (by increasing its volatility under high vacuum) shifts the equilibrium to the right and thus lowers T_{SE}.

In contrast, neat dihexadecyl disulfide and HDT@AuNPs exhibited similar mass loss behavior when analyzed using TGA. Furthermore, under high vacuum, the T_{SE} of HDT@AuNP was not notably different to that of particles under ambient pressure. These results are a consequence of the much lower volatility of the dihexadecyl disulfide (compared to dibutyl disulfide).

These findings, along with the observations made by DSC, indicate that the T_{SE} of AuNPs stabilized using alkanethiols is controlled primarily by the volatility of the resultant disulfide species.

Author Contributions

Conceptualisation: P.K.S., A.A., A.M.M.; Formal analysis: P.K.S.; Investigation: P.K.S., A.A.; Writing – original draft preparation: P.K.S., M.B.C., A.M.M.; Writing – review & editing: P.K.S., A.M.M.

Conflicts of interest

"There are no conflicts to declare".

Acknowledgements

This research is supported by an Australian Government Research Training Program Scholarship. We acknowledge the Advanced Materials Characterisation Facility (AMCF) of Western Sydney University for access to its instrumentation and staff. In particular, we thank Dr Laurel George and Dr Daniel Fanna. We acknowledge Professor James Brown, UTS, for assistance with statistical analysis and Mr Greg Delsanto, UTS science workshop, for access to equipment. Dr Angus Gentle is acknowledged for assistance with LabView software.

References

1. M. D'Acunto, P. Cioni, E. Gabellieri and G. Presciuttini, *Nanotechnology*, 2021, **32**, 192001.
2. K. Saha, S. S. Agasti, C. Kim, X. Li and V. M. Rotello, *Chemical Reviews*, 2012, **112**, 2739-2779.
3. P. T. Bishop, L. J. Ashfield, A. Berzins, A. Boardman, V. Buche, J. Cookson, R. J. Gordon, C. Salcianu and P. A. Sutton, *Gold Bulletin*, 2010, **43**, 181-188.
4. Y. Wu, Y. Li, P. Liu, S. Gardner and B. S. Ong, *Chemistry of Materials*, 2006, **18**, 4627-4632.
5. G. Korotcenkov, V. Brinzari and B. K. Cho, *Microchimica Acta*, 2016, **183**, 1033-1054.

6. X. Peng, G. Wan, L. Wu, M. Zeng, S. Lin and G. Wang, *Sensors and Actuators B: Chemical*, 2018, **257**, 166-177.
7. A. Buonerba and A. Grassi, *Catalysts*, 2021, **11**, 714.
8. R. Jin, C. Zeng, M. Zhou and Y. Chen, *Chemical Reviews*, 2016, **116**, 10346-10413.
9. D. Huang, F. Liao, S. Molesa, D. Redinger and V. Subramanian, *Journal of The Electrochemical Society*, 2003, **150**, G412-G417.
10. M. Falahati, F. Attar, M. Sharifi, A. A. Saboury, A. Salihi, F. M. Aziz, I. Kostova, C. Burda, P. Priecel, J. A. Lopez-Sanchez, S. Laurent, N. Hooshmand and M. A. El-Sayed, *Biochimica et Biophysica Acta (BBA) - General Subjects*, 2019, DOI: 10.1016/j.bbagen.2019.129435, 129435.
11. J. V. Alemán, A. V. Chadwick, J. He, M. Hess, K. Horie, R. G. Jones, P. Kratochvíl, I. Meisel, I. Mita, G. Moad, S. Penczek and R. F. T. Stepto, *Pure and Applied Chemistry*, 2007, **79**, 1801-1829.
12. S. Arcidiacono, N. R. Bieri, D. Poulikakos and C. P. Grigoropoulos, *International Journal of Multiphase Flow*, 2004, **30**, 979-994.
13. M. José-Yacamán, C. Gutierrez-Wing, M. Miki, D. Q. Yang, K. N. Piyakis and E. Sacher, *The Journal of Physical Chemistry B*, 2005, **109**, 9703-9711.
14. Y. Chen, R. E. Palmer and J. P. Wilcoxon, *Langmuir*, 2006, **22**, 2851-2855.
15. F. Ruffino, V. Torrisi and M. G. Grimaldi, *Physica E: Low-dimensional Systems and Nanostructures*, 2015, **74**, 388-399.
16. K. Lehtinen and M. Zachariah, *Journal of Aerosol Science - J AEROSOL SCI*, 2002, **33**, 357-368.
17. C. Zhu, S. Liang, E. Song, Y. Zhou, W. Wang, F. Shan, Y. Shi, C. Hao, K. Yin, T. Zhang, J. Liu, H. Zheng and L. Sun, *Nature Communications*, 2018, **9**, 421.
18. M. A. van Huis, L. T. Kunneman, K. Overgaag, Q. Xu, G. Pandraud, H. W. Zandbergen and D. Vanmaekelbergh, *Nano Letters*, 2008, **8**, 3959-3963.
19. H.-G. Liao, L. Cui, S. Whitelam and H. Zheng, *Science*, 2012, **336**, 1011-1014.
20. P. Guo and Y. Gao, *Physical Review Letters*, 2020, **124**, 066101.
21. Q. Yao, X. Yuan, V. Fung, Y. Yu, D. T. Leong, D.-e. Jiang and J. Xie, *Nature Communications*, 2017, **8**, 927.
22. S. Kundu, K. Das and O. Konovalov, *AIP Advances*, 2013, **3**, 092130.
23. R. Ristau, R. Tiruvalam, P. L. Clasen, E. P. Gorskowski, M. P. Harmer, C. J. Kiely, I. Hussain and M. Brust, *Gold Bulletin*, 2009, **42**, 133-143.
24. T. Hayashi, K. Wakamatsu, E. Ito and M. Hara, *Journal of Physical Chemistry C*, 2009, **113**, 18795-18799.
25. B. Yan, Z. J. Zhu, O. R. Miranda, A. Chompoosor, V. M. Rotello and R. W. Vachet, *Analytical and Bioanalytical Chemistry*, 2010, **396**, 1025-1035.
26. J. R. Casanova-Moreno and D. Bizzotto, *Langmuir*, 2013, **29**, 2065-2074.
27. W. H. Mulder, J. J. Calvente and R. Andreu, *Langmuir*, 2001, **17**, 3273-3280.
28. N. D. Aagaard, J. C. Azcárate, J. Olmos-Asar, M. M. Mariscal, J. Solla-Gullón, E. Zelaya and M. H. Fonticelli, *The Journal of Physical Chemistry C*, 2020, **124**, 22591-22600.
29. L. J. Cristina, G. Ruano, R. Salvarezza and J. Ferrón, *Journal of Physical Chemistry C*, 2017, **121**, 27894-27904.
30. E. Ito, H. Kang, D. Lee, J. B. Park, M. Hara and J. Noh, *Journal of Colloid and Interface Science*, 2013, **394**, 522-529.
31. S. R. King, S. Shimmon, D. D. Totonjian and A. M. McDonagh, *Journal of Physical Chemistry C*, 2017, **121**, 13944-13951.
32. J. R. Reimers, M. J. Ford, A. Halder, J. Ulstrup and N. S. Hush, *Proceedings of the National Academy of Sciences of the United States of America*, 2016, **113**, E1424-E1433.
33. E. Ito, J. Noh and M. Hara, *Chemical Physics Letters*, 2008, **462**, 209-212.
34. A. Shivhare, D. M. Chevrier, R. W. Purves and R. W. J. Scott, *Journal of Physical Chemistry C*, 2013, **117**, 20007-20016.
35. B. L. Smith and J. E. Hutchison, *Journal of Physical Chemistry C*, 2013, **117**, 25127-25137.
36. A. Tlahuice-Flores, U. Santiago, D. Bahena, E. Vinogradova, C. V. Conroy, T. Ahuja, S. B. H. Bach, A. Ponce, G. Wang, M. José-Yacamán and R. L. Whetten, *The Journal of Physical Chemistry A*, 2013, **117**, 10470-10476.
37. J. E. Martin, J. Odinek, J. P. Wilcoxon, R. A. Anderson and P. Provencio, *Journal of Physical Chemistry B*, 2003, **107**, 430-434.
38. A. Gupta, S. Mandal, M. Katiyar and Y. N. Mohapatra, *Thin Solid Films*, 2012, **520**, 5664-5670.
39. S.-R. King, J. Massicot and A. McDonagh, *Metals*, 2015, **5**, 1454-1461.
40. M. Brust, M. Walker, D. Bethell, D. J. Schiffrin and R. Whyman, *Journal of the Chemical Society, Chemical Communications*, 1994, DOI: 10.1039/C39940000801, 801-802.
41. R. H. Terrill, T. A. Postlethwaite, C.-h. Chen, C.-D. Poon, A. Terzis, A. Chen, J. E. Hutchison, M. R. Clark and G. Wignall, *Journal of the American Chemical Society*, 1995, **117**, 12537-12548.
42. M. J. Hostetler, J. E. Wingate, C.-J. Zhong, J. E. Harris, R. W. Vachet, M. R. Clark, J. D. Londono, S. J. Green, J. J. Stokes, G. D. Wignall, G. L. Glish, M. D. Porter, N. D. Evans and R. W. Murray, *Langmuir*, 1998, **14**, 17-30.
43. A. Badia, W. Gao, S. Singh, L. Demers, L. Cuccia and L. Reven, *Langmuir*, 1996, **12**, 1262-1269.
44. Z. Wu, C. Gayathri, R. R. Gil and R. Jin, *Journal of the American Chemical Society*, 2009, **131**, 6535-6542.
45. H. Qian, M. Zhu, C. Gayathri, R. R. Gil and R. Jin, *ACS Nano*, 2011, **5**, 8935-8942.
46. M. J. Coutts, M. B. Cortie, M. J. Ford and A. M. McDonagh, *The Journal of Physical Chemistry C*, 2009, **113**, 1325-1328.
47. D. Huang, F. Liao, S. Molesa, D. Redinger and V. Subramanian, *Journal of The Electrochemical Society*, 2003, **150**.
48. J. E. Martin, J. Odinek, J. P. Wilcoxon, R. A. Anderson and P. Provencio, *The journal of physical chemistry. B*, 2003, **107**, 430-434.
49. A. Gupta, S. Mandal, M. Katiyar and Y. N. Mohapatra, *Thin solid films*, 2012, **520**, 5664-5670.
50. A. Tlahuice-Flores, R. L. Whetten and M. Jose-Yacaman, *The Journal of Physical Chemistry C*, 2013, **117**, 20867-20875.
51. M.-L. Wang and Y.-H. Tseng, *Reaction Kinetics and Catalysis Letters*, 2004, **82**, 81-87.

